ACS APPLIED MATERIALS & INTERFACES

Research Article

www.acsami.org

Half-Metallic Ferromagnetism and Surface Functionalization-Induced Metal–Insulator Transition in Graphene-like Two-Dimensional Cr_2C Crystals

Chen Si,[†] Jian Zhou,[†] and Zhimei Sun*[,†,‡]

[†]School of Materials Science and Engineering and [‡]Center for Integrated Computational Materials Engineering, International Research Institute for Multidisciplinary Science, Beihang University, Beijing 100191, China

Supporting Information

ABSTRACT: Graphene-like two-dimensional materials have garnered tremendous interest as emerging device materials for nanoelectronics due to their remarkable properties. However, their applications in spintronics have been limited by the lack of intrinsic magnetism. Here, using hybrid density functional theory, we predict ferromagnetic behavior in a graphene-like two-dimensional Cr_2C crystal that belongs to the MXenes family. The ferromagnetism, arising from the itinerant Cr d electrons, introduces intrinsic half-metallicity in Cr_2C MXene, with the half-metallic gap as large as 2.85 eV. We also demonstrate a ferromagnetic–antiferromagnetic transition accompanied by a metal to insulator transition in Cr_2C, caused by surface functionalization with F, OH, H, or Cl groups. Moreover, the energy gap of the antiferromagnetic insulating state is controllable by changing the type of functional groups. We further point out that the localization of Cr d electrons induced by the surface functionalization is responsible for the ferromagnetic–antiferromagnetic and metal to insulator transitions. Our results highlight a new promising material with tunable magnetic and electronic properties toward nanoscale spintronics and electronics applications.

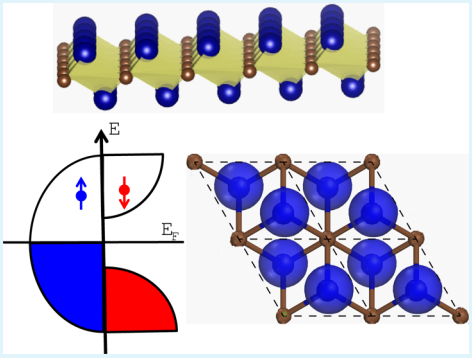

KEYWORDS: *MXene, half-metallicity, ferromagnetism, functionalization, spintronics*

I. INTRODUCTION

The discovery of graphene has spurred a surge in the study of two-dimensional (2D) materials during the past decade. Due to the dimension and size reduction and the resultant quantum effects, 2D crystals have shown many intriguing properties that are not found in their bulk counterparts,[1,2] which are hence considered as cornerstones of the future nanoscale electronics and spintronics.[3,4] Although more and more 2D crystals have been produced experimentally, the vast majority of them are nonmagnetic. Thus, the pursuit of tunable magnetism in 2D crystals has been a persistent goal for a long time.[5−8] In graphene and monolayer transition metal dichalcogenides, several ideas have been proposed to induce the magnetic moments and orderings, such as depositing magnetic adatoms on the surface[9−11] and introducing specific defects[5,6] or edges.[12−14] However, the experimental realization remains challenging: for example, the clustering of the adatoms is always inevitable,[15] and the edge morphology and defect type are not well controllable.[16] Another important property highly desirable for 2D materials, especially for their electronics applications, is the bandgap tunability, which would allow great flexibility in design and optimization of 2D-materials-based devices such as p−n junctions, transistors, photodiodes, and lasers. Though various methods for opening/tuning the gap of 2D material have been developed that include size quantization,[17] chemical functionalization,[18] strain engineering,[19] electric field control,[20] and so on, the controllable modulation of the gap is somewhat tough and bandgap engineering is still one of the hottest subjects in the field of 2D materials.

Recently, a new family of 2D early transition metal carbides and/or nitrides labeled "MXenes" has been synthesized by the extraction of "A" layers from MAX phases, which are layered ternary carbides and carbonitrides with a general formula $M_{n+1}AX_n$ (n = 1, 2, 3), where M is an early transition metal, A is mainly a group 13 or 14 element, and X is carbon and/or nitrogen.[21] The structure of the MAX phase is comprised of stacks of "$M_{n+1}X_n$" layers interleaved with "A" layers.[22,23] The A layers can be chemically etched without disrupting M−X bonds, and then the resulting weakly bonded "$M_{n+1}X_n$" layers can be readily exfoliated into MXenes.[21] To date, the MXenes family has included Ti_3C_2, Ti_2C, V_2C, Nb_2C, Ta_4C_3, Nb_4C_3, Ti_3CN, $(Ti_{0.5}Nb_{0.5})_2C$, and $(V_{0.5}Cr_{0.5})_3C_2$.[21] Moreover, because there are over 70 known MAX phases, many more MXenes are expected to be synthesized experimentally. Since their discovery, MXenes have attracted increasing attention,[24−28] showing tremendous promise for applications in electrode materials, sensors, catalysis, and electrochemical energy storage.[29−33]

Received: June 18, 2015
Accepted: July 23, 2015
Published: July 23, 2015

DOI: 10.1021/acsami.5b05401
ACS Appl. Mater. Interfaces 2015, 7, 17510−17515

In this work, using hybrid density functional theory calculations, we predict a half-metallic ferromagnet in the family of MXenes, Cr_2C MXene, which is expected to be produced by selectively etching Al atoms from the MAX phase Cr_2AlC, similar to Ti_2C and V_2C from Ti_2AlC and V_2AlC, respectively. The ferromagnetism in Cr_2C MXene is arising from the itinerant Cr d electrons which are 100% spin-polarized around the Fermi surface. And the half-metallic gap is as large as 2.85 eV. We also find that, after surface functionalization with F, OH, H, or Cl groups, the Cr_2C MXene will undergo a metal to insulator transition which is accompanied by a ferromagnetic (FM)−antiferromagnetic (AFM) transition. Moreover, the energy gap in the AFM state is controllable by changing the type of surface functionalization. We further point out that the localization of Cr d electrons induced by the functionalization is responsible for the FM−AFM and metal to insulator transitions. Our results highlight a promising material in the MXenes family, with tunable magnetic and electronic properties, extending the potential applications of MXenes into spintronics and electronics.

II. MODELS AND METHODS

Our calculations are performed in the framework of density functional theory as implemented in the Vienna *ab initio* simulation package (VASP).[34] The projector augmented wave (PAW) potential is used with the plane-wave cutoff energy set as 400 eV. The Heyd−Scuseria−Ernzerhof (HSE) screened Coulombic hybrid density functional[35] is used to describe the electron correlation effects in the structural optimizations as well as in the static calculations. The system is modeled by a pristine or functionalized Cr_2C MXene single layer and a vacuum region more than 15 Å to avoid interaction between neighboring slabs. The Brillouin zone is integrated with a 20 × 20 × 1 *k* mesh. All of the structures are fully relaxed until the remaining force acting on each atom is less than 0.01 eV/Å.

III. RESULTS AND DISCUSSION

Figure 1a shows the lattice structure of Cr_2C MXene. It is comprised of triple layers where a C atomic layer is sandwiched between two Cr layers. From its top view, we can see the Cr atoms are arranged in hexagonal structure, where the Cr atoms in two different layers form two triangular sublattices. It is found that Cr_2C MXene energetically favors the spin-polarized ground state, and the energy difference between the spin-polarized and spin-unpolarized states is large, which is about 2.53 eV per unit cell containing two Cr atoms and one C atom. In the spin-polarized ground state, the equilibrium lattice constant is calculated to be 3.14 Å (see Figure 1b), with the thickness of the Cr_2C triple layers (h) and the Cr−C bond length being 2.10 and 2.12 Å, respectively. The structural stability of Cr_2C MXene is also verified by the phonon spectra calculations where no negative frequency phonon is found at any wave vector [see the Supporting Information]. The total magnetic moment per unit cell is calculated to be 8 μ_B, mainly contributed to by the two Cr atoms.

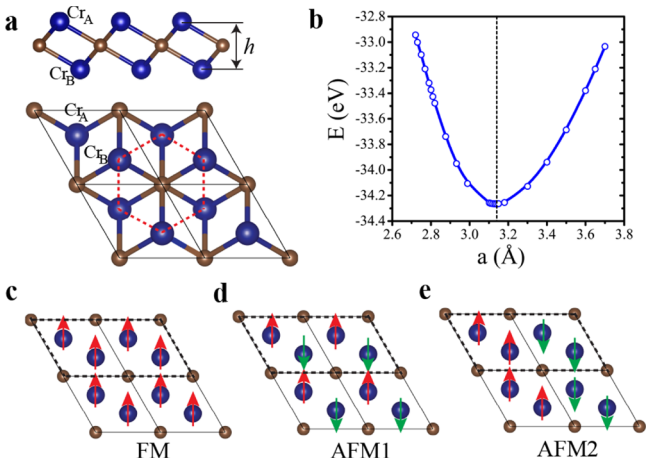

Figure 1. (a) Side and top views of Cr_2C MXene lattice. Blue and brown balls represent Cr and C atoms, respectively. The unit cell of Cr_2C MXene contains two Cr atoms (Cr_A and Cr_B) and one C atom. (b), Variation of total energy of Cr_2C MXene with the lattice constant. (c−e), Schematics of three different magnetic structures: FM, AFM1, and AFM2. The dashed line outlines the 2 × 1 supercell used for total energy calculations.

In order to find the preferred magnetic coupling between the Cr atoms, we use a 2 × 1 supercell that contains four Cr atoms. Depending on the initial conditions of the self-consistent calculations, we obtain three stable magnetic structures: FM (Figure 1c), AFM1 (Figure 1d), and AFM2 (Figure 1e). (Note that the AFM1 and AFM2 structures shall not be considered as realistic AFM orderings. They are studied only for obtaining the magnetic interaction.) Taking the energy of the FM structure as the reference, the relative energies of the AFM1 and AFM2 structures are 0.36 and 1.06 eV, respectively. The exchange interaction can be conveniently studied by mapping the total energies of the systems with different magnetic orderings to a Heisenberg model with the nearest- and next-nearest-neighbor couplings J_1 and J_2:

$$H = -\sum_{i,j} J_1 S_i \cdot S_j - \sum_{k,l} J_2 S_k \cdot S_l \quad (1)$$

where S_i is the net spin at the Cr sites i and (i, j) and (k, l) are the nearest site pairs and next-nearest site pairs, respectively. Based on this model, the energy difference between the FM and the AFM1 phases is $E^{AFM1}-E^{FM} = 12J_1S^2$, and the energy difference between the FM and AFM2 phases is $E^{AFM2}-E^{FM} = (4J_1 + 16J_2)S^2$. Then the exchange coupling parameters are calculated to be J_1 = 7.4 meV and J_2 = 14.7 meV. Their positive values clearly indicate that Cr_2C MXene prefers FM coupling. Moreover, based on *ab initio* molecular dynamics simulations, we further find the magnetic state of Cr_2C could survive at room temperature (see the Supporting Information).

Having studied the magnetic ground state of Cr_2C MXene, we now turn to its electronic structure. As shown in Figure 2a, the most striking property of this band structure is the half-metallicity, i.e, a metallic character found for the majority-spin electrons while an insulating nature is found for the minority-spin electrons. Thus, the charge transport is dominated by the majority-spin electrons, and the electrical current in such a system should be completely spin-polarized. The half-metallic gap, defined as the difference between the Fermi level and topmost occupied minority-spin band,[36] is as large as 2.85 eV, suggesting that the 100% spin-filter efficiency can be maintained in a broad bias range. It is stressed that the half-metallicity in Cr_2C MXene is completely intrinsic, in contrast to other low-dimensional materials, such as graphene or boron nitride nanoribbon,[12,36−38] C/BN heterostructures,[39,40] and MoS_2[41] and $MnPSe_3$ nanosheets,[42] where the presence of half-metallicity needs either a strong external electric field or the carefully selective doping. Such an intriguing physical property, half-metallic ferromagnetism, makes Cr_2C MXene an attractive candidate for nanoscale spintronics applications. It is worth

DOI: 10.1021/acsami.5b05401
ACS Appl. Mater. Interfaces 2015, 7, 17510−17515

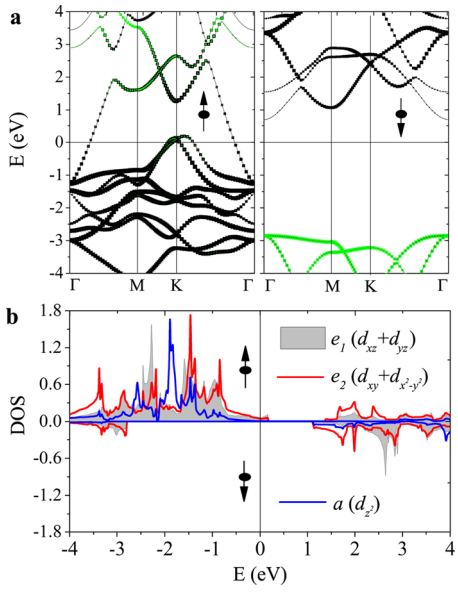

Figure 2. (a) Band structure for Cr_2C MXene. The black and green squares represent the weights of the Cr d and C p orbitals, respectively. (b), Partial density of states of Cr d orbitals. The Fermi level in a and b is set to zero.

mentioning that Cr_2C MXene is the first reported half-metallic ferromagnet among the MXenes family. Even though its ferromagnetic property was concluded by simply comparing the energies of the ferromagnetic and nonmagnetic states in a recent work by Khazaei et al., the half-metallicity of 2D Cr_2C was not discovered therein, probably due to the lack of extensive study on electronic structures.[43]

Another remarkable feature of the band structure is the strongly dispersing bands crossing the Fermi level (E_F), which provides the clues to the basic mechanism for the ferromagnetic metal behavior. The atomic and orbital resolved characters of the energy bands show a predominant contribution of Cr d orbitals to the dispersing bands that cross the E_F (see Figure 2a). This means the Cr d electronic states around the E_F are itinerant. According to the Stoner theory, the itinerant d electrons would favor ferromagnetism.[44] In Cr_2C MXene, each Cr^{2+} ion has a closed shell Ar core and four additional 3d electrons. Under the C_{3v} symmetry of the crystal field, the 3d orbitals of Cr split into a single a (d_{z^2}) orbital and two 2-fold degenerate e_1 (d_{xz} + d_{yz}) and e_2 (d_{xy} + $d_{x^2-y^2}$) orbitals. Because of the large exchange splitting of the Cr 3d orbitals, the four 3d electrons only occupy the majority-spin channel, resulting in an energy gap between the occupied C p orbitals and the empty Cr d orbitals in the minority-spin channel straddling the Fermi energy (see Figure 2a). Then why is the majority-spin channel metallic? Here we point out that this is associated with the nonlocalized nature of the d orbitals. Figure 2b displays the projected density of states (PDOS) of a, e_1, and e_2 orbitals. It is clearly seen that the a, e_1, and e_2 orbitals are not localized, showing wide peaks and overlapping with each other. Consequently, in the majority-spin channel, all of them are fractionally occupied, resulting in the appearance of the metallicity.

At present, the main synthesis method for MXenes is etching Al from MAX phases in the hydrofluoric acid or a solution of lithium fluoride and hydrochloric acid,[21,25] making the termination of MXenes surfaces by OH or F groups possible.[21]

It is widely known that the surface functionalization is one of the main methods to manipulate the physical and chemical properties of 2D materials.[18,45] Thus, we have also studied the functionalized Cr_2C MXene, i.e., Cr_2C MXene with surface fully terminated by possible functional groups, denoted by a general formula of Cr_2CT_2, where T stands for surface terminations (F, OH, H, or Cl).

Parts a and b of Figure 3 show the lattice structure of Cr_2CF_2. It is determined by considering and comparing all

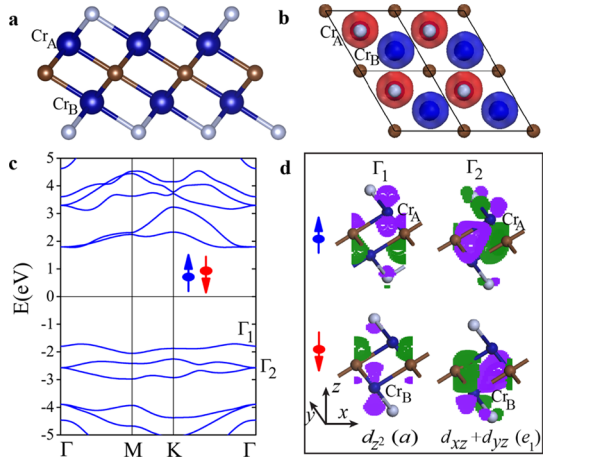

Figure 3. (a, b) Side and top views of optimized structure of Cr_2CF_2. Blue, brown, and gray balls denote the Cr, C, and F atoms, respectively. The spin density ($\rho_\uparrow-\rho_\downarrow$) map of Cr_2CF_2 is also shown in b. The blue and red colors represent opposite spin orientations: spin up and spin down. (c) Band structure of Cr_2CF_2 under the AFM ground state. The blue lines are for the majority-spin and the red lines are for the minority-spin, where the blue lines completely overlap with the red lines. (d) The wave function for the three highest valence states at the Γ point (Γ_1 and doubly degenerate Γ_2) in the majority- and minority-spin channel. The Γ_1 and Γ_2 states are mainly contributed to by the Cr d_{z^2} (a) and d_{xz} + d_{yz} (e_1) orbitals, respectively. The small contribution from C atoms is due to the weak covalence of the Cr_2CF_2 system.

possible adsorption configurations of F atoms on the surface of Cr_2C MXene. One can see that on both sides of Cr_2C, F atoms are located above the hollow sites of three neighboring C atoms, pointing to the Cr atoms in the nonadjacent Cr layer. We stress that the fluorination will not break the structural stability of the system: by calculating the phonon spectra of Cr_2CF_2, we find that all of the phonon frequencies are positive (see the Supporting Information). Moreover, after fluorination, the magnetic moments on the Cr atoms do not vanish. In order to explore the magnetic ground state of Cr_2CF_2, we use a 2 × 2 supercell and consider the nonmagnetic (NM) structure, the FM structure, and all of the possible AFM magnetic structures. We find the ground state is AFM where all of the nearest Cr neighbors have antiparallel spins (corresponding to the AFM1 structure in Figure 1e). This AFM state is more stable than the FM state by an energy difference of 0.60 eV per unit cell containing two Cr atoms. Figure 3b shows the spin density map of Cr_2CF_2 at the AFM ground state, where one can clearly see that the magnetic moments are mainly contributed to by the Cr atoms and the nearest Cr atoms antiferromagnetically couple with each other. The local magnetic moment on each Cr atom is about 3 μ_B.

The band structure of Cr_2CF_2 is shown in Figure 3c, where semiconducting behaviors are found for both the majority- and

DOI: 10.1021/acsami.5b05401
ACS Appl. Mater. Interfaces 2015, 7, 17510−17515

minority-spin electrons. The band gap is indirect, about 3.49 eV, much larger than the monolayer MoS_2 (1.8 eV)[46] and phosphorene (2.1 eV)[47] but smaller than the *h*-BN single layer (5.97 eV)[48] and graphane (5.4 eV).[18] It is also noted that the three highest valence bands, mainly contributed to by Cr d orbitals, are nearly dispersionless with very narrow bandwidth. This distinctly indicates the localized character of d electrons, which we will show is a dominant reason for the insulating behavior of Cr_2CF_2 in the following. The Cr atom in Cr_2CF_2 is under the D_{3d} symmetry that split 3d orbitals into a single a (d_{z^2}) orbital and two doubly degenerate e_1 (d_{xz} + d_{yz}) and e_2 (d_{xy} + $d_{x^2-y^2}$) orbitals. In its 3+ valence state, each Cr ion has three 3d electrons. Due to the large exchange splitting of Cr d orbitals, the three 3d electrons only occupy one spin channel. Moreover, because of the localized character of the d orbitals, the e_1 and a orbitals in one spin channel are completely occupied in sequence, while the e_2 orbitals are unoccupied, resulting in the formation of semiconductivity. The occupation of e_1 and a orbitals could be verified by the wave function of the highest valence states at the Γ point. As shown in Figure 3d, in the majority channel, at the Γ point, the highest occupied states (Γ_1) are mainly contributed to by the Cr_A d_{z^2} (a) orbital, and the second highest states (Γ_2), which are 2-fold degenerate, are mainly contributed to by the Cr_A d_{xz} + d_{yz} (e_1) orbitals. Correspondingly, in the minority-spin channel, Γ_1 and Γ_2 are mainly contributed to by Cr_B d_{z^2} (a) and d_{xz} + d_{yz} (e_1) orbitals, respectively.

After knowing the electron configuration of Cr^{3+} ion in Cr_2CF_2, it is not surprising that Cr^{3+} ions couple antiferromagnetically. This is because the e_1 and a orbitals of a Cr^{3+} ion in one spin channel are fully occupied; virtual hopping is allowed in the AFM arrangement but not allowed in the FM configuration (see Figure 4a), resulting in a lower energy AFM state.

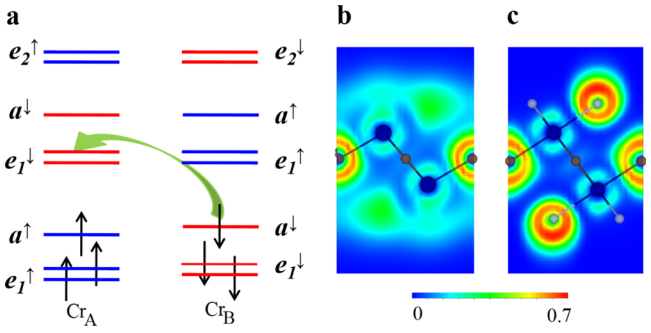

Figure 4. (a) Schematic of the exchange mechanism for Cr_2CF_2. The e_1 and a orbitals of a Cr^{3+} ion are occupied in one spin channel, and thus virtual hopping results in the AFM arrangement. (b, c) ELF maps of Cr_2C and Cr_2CF_2, respectively.

So far, we have shown that, from Cr_2C to Cr_2CF_2, fluorination induces an interesting metal to insulator transition which is accompanied by a FM−AFM transition. We have also pointed out that the completely different electronic and magnetic properties of Cr_2C and Cr_2CF_2 are closely related to different characteristics of their d orbitals: the former has itinerant d orbitals, while the latter has localized d orbitals. This could be qualitatively reflected by their electron-localization function (ELF). As shown in Figure 4b,c, a delocalized ELF feature for Cr_2C is in contrast to a localized ELF feature for Cr_2CF_2.

Other functionalized MXenes, $Cr_2C(OH)_2$, Cr_2CH_2, and Cr_2CCl_2, show lattice structures and antiferromagnetic ground states similar to those of Cr_2CF_2. All of them are semiconductors, with the sizes of energy gaps being 1.43 eV for $Cr_2C(OH)_2$, 1.76 eV for Cr_2CH_2, 2.56 eV for Cr_2CCl_2, and 3.49 eV for Cr_2CF_2 (see Figure 5). That is to say, by choosing

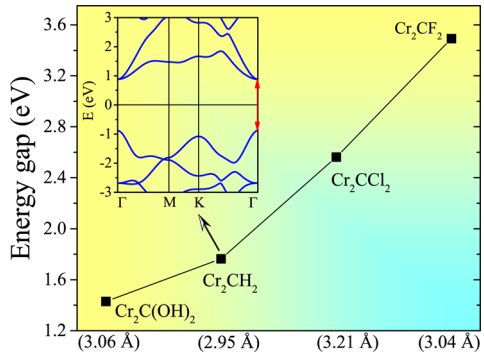

Figure 5. Energy gap of Cr_2CT_2 (T = F, OH, H, or Cl) MXenes. The numbers in the brackets under the *x* axis are the lattice constants for corresponding Cr_2CT_2 MXenes. Inset: Band structure of Cr_2CH_2 with the direct gap at the Γ point highlighted by a red arrow. The Fermi level is set to zero.

different surface functional groups, one can change the metallic Cr_2C MXene into a semiconductor and tune the band gap to different regimes. Most remarkably, Cr_2CH_2 has a direct band gap, with the conduction band minimum and the valence band maximum both located at the Γ point, as shown in the inset of Figure 5. The direct gap that facilitates efficient light emission, makes Cr_2CH_2 an attractive material for the applications in optoelectronic nanodevices. Earlier works have successively found six types of terminated MXenes which are semiconductors: Ti_2CO_2, Zr_2CO_2, Hf_2CO_2, Sc_2CO_2, $Sc_2C(OH)_2$, and Sc_2CF_2.[43,49,50] The finding of semiconducting Cr_2CT_2 (T = F, OH, H, or Cl), further expands the semiconducting MXenes family. Finally, we should stress the significant difference between Cr_2CT_2 and the six other types of semiconducting MXenes mentioned earlier: the former are magnetic, while the latter are nonmagnetic.

IV. CONCLUSIONS

In conclusion, we have studied the electronic and magnetic properties of Cr_2C MXene based on hybrid density functional theory calculations. We show that Cr_2C MXene exhibits half-metallic ferromagnetic behavior with a large half-metallic gap of 2.85 eV. The ferromagnetism is arising from the itinerant Cr d electrons which are 100% spin-polarized around the Fermi surface. We also demonstrate a FM−AFM transition in Cr_2C MXene caused by surface functionalization with F, H, OH, or Cl groups, which is accompanied by a metal to insulator transition. It is noted that the size of the band gap in the AFM insulating state is controllable by selecting different functional groups. And hydrogenation can open a direct band gap in Cr_2C MXene. We further point out that the functionalization induced localization of Cr d electrons is the underlying mechanism for the FM−AFM and metal to insulator transitions. Our results demonstrate the potential for the utilization of Cr_2C MXene in innovative spintronics and electronics devices.

DOI: 10.1021/acsami.5b05401
ACS Appl. Mater. Interfaces 2015, 7, 17510−17515

■ ASSOCIATED CONTENT

Supporting Information

The Supporting Information is available free of charge on the ACS Publications website at DOI: 10.1021/acsami.5b05401.

Phonon spectra and molecular dynamics simulations for the Cr_2C MXene (PDF)

■ AUTHOR INFORMATION

Corresponding Author

*E-mail: zmsun@buaa.edu.cn.

Notes

The authors declare no competing financial interest.

■ ACKNOWLEDGMENTS

We acknowledge the fruitful discussions with Bin Shao and Pengcheng Chen. This work is supported by the National Natural Science Foundation for Distinguished Young Scientists of China (Grant 51225205) and the National Natural Science Foundation of China (Grant 61274005).

■ REFERENCES

(1) Xu, M.; Liang, T.; Shi, M.; Chen, H. Graphene-Like Two-Dimensional Materials. *Chem. Rev.* **2013**, *113*, 3766−3798.

(2) Si, C.; Liu, Z.; Duan, W.; Liu, F. First-Principles Calculations on the Effect of Doping and Biaxial Tensile Strain on Electron-Phonon Coupling in Graphene. *Phys. Rev. Lett.* **2013**, *111*, 196802.

(3) Novoselov, K. S.; Fal'ko, V. I.; Colombo, L.; Gellert, P.; Schwab, M.; Kim, K. A Roadmap for Graphene. *Nature* **2012**, *490*, 192−200.

(4) Wang, Q. H.; Kalantar-Zadeh, K.; Kis, A.; Coleman, J. N.; Strano, M. S. Electronics and Optoelectronics of Two-dimensional Transition Metal Dichalcogenides. *Nat. Nanotechnol.* **2012**, *7*, 699−712.

(5) Yazyev, O. V. Emergence of Magnetism in Graphene Materials and Nanostructures. *Rep. Prog. Phys.* **2010**, *73*, 056501.

(6) Zhang, Z.; Zou, X.; Crespi, V. H.; Yakobson, B. I. Intrinsic Magnetism of Grain Boundaries in Two-Dimensional Metal Dichalcogenides. *ACS Nano* **2013**, *7*, 10475−10481.

(7) Ma, Y.; Dai, Y.; Guo, M.; Niu, C.; Zhu, Y.; Huang, B. Evidence of the Existence of Magnetism in Pristine VX_2 Monolayers (X = S, Se) and Their Strain-Induced Tunable Magnetic Properties. *ACS Nano* **2012**, *6*, 1695−1701.

(8) Du, A.; Sanvito, S.; Smith, S. C. First-Principles Prediction of Metal-Free Magnetism and Intrinsic Half-Metallicity in Graphitic Carbon Nitride. *Phys. Rev. Lett.* **2012**, *108*, 197207.

(9) Sevinçli, H.; Topsakal, M.; Durgun, E.; Ciraci, S. Electronic and Magnetic Properties of 3d Transition-Metal Atom Adsorbed Graphene and Graphene Nanoribbons. *Phys. Rev. B: Condens. Matter Mater. Phys.* **2008**, *77*, 195434.

(10) Sui, X.; Si, C.; Shao, B.; Zou, X.; Wu, J.; Gu, B. L.; Duan, W. Tunable Magnetism in Transition Metal Decorated Phosphorene. *J. Phys. Chem. C* **2015**, *119*, 10059−10063.

(11) Li, Y.; Chen, X.; Zhou, G.; Duan, W.; Kim, Y.; Kim, M.; Ihm, J. Trends in Charge Transfer and Spin Alignment of Metallocene on Graphene. *Phys. Rev. B: Condens. Matter Mater. Phys.* **2011**, *83*, 195443.

(12) Son, Y.-W.; Cohen, M. L.; Louie, S. G. Half-metallic Graphene Nanoribbons. *Nature* **2006**, *444*, 347−349.

(13) Li, Y.; Zhou, Z.; Zhang, S.; Chen, Z. MoS_2 Nanoribbons: High Stability and Unusual Electronic and Magnetic Properties. *J. Am. Chem. Soc.* **2008**, *130*, 16739−16744.

(14) Yu, D.; Lupton, E. M.; Gao, H.; Zhang, C.; Liu, F. A Unified Geometric Rule for Designing Nanomagnetism in Graphene. *Nano Res.* **2008**, *1*, 497−501.

(15) Subrahmanyam, K.; Manna, A. K.; Pati, S. K.; Rao, C. A Study of Graphene Decorated with Metal Nanoparticles. *Chem. Phys. Lett.* **2010**, *497*, 70−75.

(16) Banhart, F.; Kotakoski, J.; Krasheninnikov, A. V. Structural Defects in Graphene. *ACS Nano* **2011**, *5*, 26−41.

(17) Han, M. Y.; Özyilmaz, B.; Zhang, Y.; Kim, P. Energy Band-Gap Engineering of Graphene Nanoribbons. *Phys. Rev. Lett.* **2007**, *98*, 206805.

(18) Lebegue, S.; Klintenberg, M.; Eriksson, O.; Katsnelson, M. Accurate Electronic Band Gap of Pure and Functionalized Graphane from GW Calculations. *Phys. Rev. B: Condens. Matter Mater. Phys.* **2009**, *79*, 245117.

(19) Scalise, E.; Houssa, M.; Pourtois, G.; Afanas'ev, V.; Stesmans, A. Strain-Induced Semiconductor to Metal Transition in the Two-Dimensional Honeycomb Structure of MoS_2. *Nano Res.* **2012**, *5*, 43−48.

(20) Zhang, Y.; Tang, T.-T.; Girit, C.; Hao, Z.; Martin, M. C.; Zettl, A.; Crommie, M. F.; Shen, Y. R.; Wang, F. Direct Observation of a Widely Tunable Bandgap in Bilayer Graphene. *Nature* **2009**, *459*, 820−823.

(21) Naguib, M.; Mochalin, V. N.; Barsoum, M. W.; Gogotsi, Y. Two-Dimensional Materials: 25th Anniversary Article: MXenes: A New Family of Two-Dimensional Materials. *Adv. Mater.* **2014**, *26*, 992−1005.

(22) Sun, Z.; Ahuja, R.; Li, S.; Schneider, J. M. Structure and bulk modulus of M_2AlC (M = Ti, V, and Cr). *Appl. Phys. Lett.* **2003**, *83*, 899−901.

(23) Guo, Z.; Zhu, L.; Zhou, J.; Sun, Z. Microscopic Origin of MXenes Derived from Layered MAX Phases. *RSC Adv.* **2015**, *5*, 25403−25408.

(24) Tang, Q.; Zhou, Z.; Shen, P. Are MXenes Promising Anode Materials for Li Ion Batteries? Computational Studies on Electronic Properties and Li Storage Capability of Ti_3C_2 and $Ti_3C_2X_2$ (X = F, OH) Monolayer. *J. Am. Chem. Soc.* **2012**, *134*, 16909−16916.

(25) Ghidiu, M.; Lukatskaya, M. R.; Zhao, M.-Q.; Gogotsi, Y.; Barsoum, M. W. Conductive Two-Dimensional Titanium Carbide 'Clay' with High Volumetric Capacitance. *Nature* **2014**, *516*, 78−81.

(26) Xie, Y.; Naguib, M.; Mochalin, V. N.; Barsoum, M. W.; Gogotsi, Y.; Yu, X.; Nam, K.-W.; Yang, X.-Q.; Kolesnikov, A. I.; Kent, P. R. Role of Surface Structure on Li-Ion Energy Storage Capacity of Two-Dimensional Transition-Metal Carbides. *J. Am. Chem. Soc.* **2014**, *136*, 6385−6394.

(27) Khazaei, M.; Arai, M.; Sasaki, T.; Estili, M.; Sakka, Y. Two-dimensional Molybdenum Carbides: Potential Thermoelectric Materials of the MXene Family. *Phys. Chem. Chem. Phys.* **2014**, *16*, 7841−7849.

(28) Guo, Z.; Zhou, J.; Si, C.; Sun, Z. Flexible Two-Dimensional $Ti_{n+1}C_n$ (n = 1,2 and 3) and Their Functionalized MXenes Predicted by Density Functional Theories. *Phys. Chem. Chem. Phys.* **2015**, *17*, 15348−15354.

(29) Peng, Q.; Guo, J.; Zhang, Q.; Xiang, J.; Liu, B.; Zhou, A.; Liu, R.; Tian, Y. Unique Lead Adsorption Behavior of Activated Hydroxyl Group in Two-Dimensional Titanium Carbide. *J. Am. Chem. Soc.* **2014**, *136*, 4113−4116.

(30) Ling, Z.; Ren, C. E.; Zhao, M.-Q.; Yang, J.; Giammarco, J. M.; Qiu, J.; Barsoum, M. W.; Gogotsi, Y. Flexible and Conductive MXene Films and Nanocomposites with High Capacitance. *Proc. Natl. Acad. Sci. U. S. A.* **2014**, *111*, 16676−16681.

(31) Lukatskaya, M. R.; Mashtalir, O.; Ren, C. E.; Dall'Agnese, Y.; Rozier, P.; Taberna, P. L.; Naguib, M.; Simon, P.; Barsoum, M. W.; Gogotsi, Y. Cation Intercalation and High Volumetric Capacitance of Two-Dimensional Titanium Carbide. *Science* **2013**, *341*, 1502−1505.

(32) Eames, C.; Islam, M. S. Ion Intercalation into Two-Dimensional Transition-Metal Carbides: Global Screening for New High-Capacity Battery Materials. *J. Am. Chem. Soc.* **2014**, *136*, 16270−16276.

(33) Hu, J.; Xu, B.; Ouyang, C.; Yang, S. A.; Yao, Y. Investigations on V_2C and V_2CX_2 (X = F, OH) Monolayer as a Promising Anode Material for Li Ion Batteries from First-Principles Calculations. *J. Phys. Chem. C* **2014**, *118*, 24274−24281.

(34) Kresse, G.; Furthmüller, J. Efficiency of Ab-Initio Total Energy Calculations for Metals and Semiconductors Using a Plane-Wave Basis Set. *Comput. Mater. Sci.* **1996**, *6*, 15−50.

(35) Heyd, J.; Scuseria, G. E.; Ernzerhof, M. Hybrid Functionals Based on a Screened Coulomb Potential. *J. Chem. Phys.* **2003**, *118*, 8207−8215.
(36) Zheng, F.; Zhou, G.; Liu, Z.; Wu, J.; Duan, W.; Gu, B.-L.; Zhang, S. Half Metallicity along the Edge of Zigzag Boron Nitride nanoribbons. *Phys. Rev. B: Condens. Matter Mater. Phys.* **2008**, *78*, 205415.
(37) Wu, M.; Wu, X.; Gao, Y.; Zeng, X. C. Materials Design of Half-Metallic Graphene and Graphene Nanoribbons. *Appl. Phys. Lett.* **2009**, *94*, 223111.
(38) Du, A.; Chen, Y.; Zhu, Z.; Amal, R.; Lu, G. Q.; Smith, S. C. Dots versus Antidots: Computational Exploration of Structure, Magnetism, and Half-Metallicity in Boron-Nitride Nanostructures. *J. Am. Chem. Soc.* **2009**, *131*, 17354−17359.
(39) Dutta, S.; Manna, A. K.; Pati, S. K. Intrinsic Half-Metallicity in Modified Graphene Nanoribbons. *Phys. Rev. Lett.* **2009**, *102*, 096601.
(40) Huang, B.; Si, C.; Lee, H.; Zhao, L.; Wu, J.; Gu, B.-L.; Duan, W. Intrinsic Half-Metallic BN-C Nanotubes. *Appl. Phys. Lett.* **2010**, *97*, 043115.
(41) Chen, Q.; Ouyang, Y.; Yuan, S.; Li, R.; Wang, J. Uniformly Wetting Deposition of Co Atoms on MoS_2 Monolayer: A Promising Two-Dimensional Robust Half-Metallic Ferromagnet. *ACS Appl. Mater. Interfaces* **2014**, *6*, 16835−16840.
(42) Li, X.; Wu, X.; Yang, J. Half-Metallicity in $MnPSe_3$ Exfoliated Nanosheet with Carrier Doping. *J. Am. Chem. Soc.* **2014**, *136*, 11065−11069.
(43) Khazaei, M.; Arai, M.; Sasaki, T.; Chung, C. Y.; Venkataramanan, N. S.; Estili, M.; Sakka, Y.; Kawazoe, Y. Novel Electronic and Magnetic Properties of Two-Dimensional Transition Metal Carbides and Nitrides. *Adv. Funct. Mater.* **2013**, *23*, 2185−2192.
(44) Capellmann, H. Theory of Itinerant Ferromagnetism in the 3-d Transition Metals. *Z. Phys. B: Condens. Matter Quanta* **1979**, *34*, 29−35.
(45) Si, C.; Liu, J.; Xu, Y.; Wu, J.; Gu, B.-L.; Duan, W. Functionalized Germanene as a Prototype of Large-Gap Two-Dimensional Topological Insulators. *Phys. Rev. B: Condens. Matter Mater. Phys.* **2014**, *89*, 115429.
(46) Mak, K. F.; Lee, C.; Hone, J.; Shan, J.; Heinz, T. F. Atomically Thin MoS_2: A New Direct-Gap Semiconductor. *Phys. Rev. Lett.* **2010**, *105*, 136805.
(47) Liang, L.; Wang, J.; Lin, W.; Sumpter, B. G.; Meunier, V.; Pan, M. Electronic Bandgap and Edge Reconstruction in Phosphorene Materials. *Nano Lett.* **2014**, *14*, 6400−6406.
(48) Watanabe, K.; Taniguchi, T.; Kanda, H. Direct-Bandgap Properties and Evidence for Ultraviolet Lasing of Hexagonal Boron Nitride Single Crystal. *Nat. Mater.* **2004**, *3*, 404−409.
(49) Xie, Y.; Kent, P. Hybrid Density Functional Study of Structural and Electronic Properties of Functionalized $Ti_{n+1}X_n$ (X= C, N) Monolayers. *Phys. Rev. B: Condens. Matter Mater. Phys.* **2013**, *87*, 235441.
(50) Lee, Y.; Cho, S. B.; Chung, Y.-C. Tunable Indirect to Direct Band Gap Transition of Monolayer Sc_2CO_2 by the Strain Effect. *ACS Appl. Mater. Interfaces* **2014**, *6*, 14724−14728.

DOI: 10.1021/acsami.5b05401
ACS Appl. Mater. Interfaces 2015, 7, 17510−17515